

A high-sensitivity 6.7 GHz methanol maser survey toward H₂O sources

Y. Xu^{1,2}, J. J. Li³, K. Hachisuka³, J. D. Pandian¹, K. M. Menten¹, C. Henkel¹

¹ Max-Planck-Institute für Radioastronomie, Auf dem Hügel 69, 53121 Bonn, Germany
e-mail: xuye@mpifr-bonn.mpg.de

² Purple Mountain Observatory, Chinese Academy of Sciences, Nanjing 210008, China

³ Shanghai Astronomical Observatory, Chinese Academy of Sciences, Shanghai 20030, China

Received date; accepted date

Abstract. We present the results of a high sensitivity survey for 6.7 GHz methanol masers towards 22 GHz water maser using the 100 m Effelsberg telescope. A total of 89 sources were observed and 10 new methanol masers were detected. The new detections are relatively faint with peak flux densities between 0.5 and 4.0 Jy. A nil detection rate from low-mass star forming regions enhances the conclusion that the masers are only associated with massive star formation. Even the faintest methanol maser in our survey, with a luminosity of $1.1 \cdot 10^{-9} L_{\odot}$ is associated with massive stars as inferred from its infrared luminosity.

Key words. masers — survey — star: formation — ISM: molecules

1. Introduction

The 5_1-6_0 A⁺ transition of methanol at 6.7 GHz produces the brightest known methanol masers. These masers are widespread in the Galaxy and more than 550 sources have been detected to date, including the compilations of Xu et al. (2003), Malyshev & Sobolev (2003) and Pestalozzi et al. (2005) and the new searches of Pandian et al. (2007) and Ellingsen (2007). The masers are not only a powerful tool of massive star-forming regions, but are also potentially useful for measuring distances using VLBI techniques, as has been demonstrated using their 12.2 GHz counterparts (Xu et al. 2006). Searches for 6.7 GHz methanol masers have been primarily targeted toward IRAS sources, OH masers, and ultracompact HII regions (e.g. Caswell et al. 1995; Walsh et al. 1997; Szymczak et al. 2000). In addition there have been a few blind surveys (Caswell et al. 1995; Ellingsen et al. 1996, Szymczak et al. 2002, Pandian et al. 2007). Unlike surveys in Southern sky, most surveys in Northern sky have a sensitivity limit of more than 1 Jy. The recent blind survey using the 305 m Arecibo radio telescope resulted in the discovery of numerous faint (< 1 Jy) methanol masers (Pandian et al. 2007).

Here, we report on the results of a sensitive survey for CH₃OH masers targeted towards H₂O maser sources, primarily in the Northern sky. Although there is no spatial correlation between 6.7 GHz CH₃OH and 22 GHz H₂O masers (Beuther et al. 2002; Breen et al. 2007), a

high detection rate of both maser types in the same star forming regions indicates that the maser bearing phases for these two species overlap (Codella & Moscadelli 2000; Szymczak et al. 2005). The goals of our survey are two-fold: to find more CH₃OH masers as astrometric targets for future VLBI observations to understand the spiral structure of the Galaxy. Further, since H₂O masers are found towards both low-mass and high-mass star forming regions, we hope to verify the exclusive association of 6.7 GHz methanol masers with massive star formation.

2. Observations

The observations were made using the Effelsberg 100 m telescope¹ in February and May 2006. The rest frequency adopted for the $5_1 - 6_0$ A⁺ transition was 6668.519 MHz (Breckenridge & Kukolich 1995). For the February observations, the spectrometer was configured to have a 10 MHz bandwidth with 4096 spectral channels yielding a spectral resolution of 0.11 km s⁻¹ and a velocity coverage of 450 km s⁻¹. In May, a bandwidth of 20 MHz was used giving a spectral resolution of 0.22 km s⁻¹ and a velocity coverage of 900 km s⁻¹. The half-power beam width was $\sim 2''$ and the telescope has an rms pointing error of 10''. The observations were made in position switched mode. The system temperature was typically around 35 K during our

¹ Based on observations with the 100-m telescope of the MPIfR (Max-Planck-Institut für Radioastronomie) at Effelsberg.

observations. The flux density scale was determined by observations of NGC7027 (Ott et al. 1994). The absolute calibration for flux density is estimated to be accurate to $\sim 10\%$. The integration time on source was typically three minutes, which resulted in a mean rms noise level of $\sim 0.1 - 0.2$ Jy in the spectra. When a source was detected, the integration time was increased to around 8 minutes (at the same position) with a velocity resolution of 0.11 km s^{-1} to obtain spectra with high signal to noise ratio.

The target sources were H_2O masers selected from the Arcetri catalog (Comoretto et al. 1990 and Brand et al. 1994), and are shown in Table 1. The sources were selected based on associations with star forming regions or HII regions, with declinations $\delta \geq -10^\circ$. This gave us a sample of 178 sources of which 17 sources may be associated with low-mass young stellar objects (YSOs) with infrared luminosities less than $10^3 L_\odot$. 154 out of 178 sources are associated with IRAS point sources. We then excluded sources that had previous detections of methanol masers, which reduced our sample size to 131 sources. Of this, we observed a total of 89 sources within our observing time constraints. For all sources, the spectrometer was centered on the velocity of peak emission of the water maser. However, the wide velocity coverage precludes the possibility of methanol masers being missed due to their velocities being significantly offset from that of the water masers.

3. Results

Our observations resulted in the discovery of 10 new methanol masers, the properties of which are listed in Table 2. Since we did not attempt to refine the position of the methanol masers using a grid of observations, the positions quoted in Table 2 could have an error as high as $\sim 1'$. The maser luminosities quoted in Table 2 are calculated from the integrated flux density assuming isotropic emission. Details of water maser sources that had non-detections of methanol masers are indicated in Table 3, which is available on-line. The peak flux densities of the methanol masers detected in our survey range from 0.5 to 4.0 Jy. Five sources are located beyond the solar circle, which is a significant addition to the number of such sources in the northern sky. It is interesting that the kinematic distance to the source 05137+3919 puts it at a distance of ~ 14 kpc from the Sun and 20 kpc from the Galactic center. This is one of the farthest methanol masers (in terms of distance from the Galactic center) in the outer Galaxy, although the uncertainties in the rotation curve at these galactrocentric radii, and peculiar motions such as that observed in W3OH (Xu et al. 2006) translate to significant uncertainties in the kinematic distance. Measuring parallax distances to sources like 05137+3919 will be useful for measuring the rotation speed of the Galaxy at large galactocentric radii.

3.1. Individual sources

The spectra of the CH_3OH masers detected in our survey are shown in Figure 1. The spectra have a velocity resolution of 0.11 km s^{-1} . Here we present notes on individual sources.

05137+3919. There are two features that are separated by about 4.5 km s^{-1} . The stronger feature is at an LSR velocity of -3.9 km s^{-1} , while the weaker feature has a flux density of only 0.35 Jy. This region is associated with a 3.6 cm continuum source (Molinari et al. 2002).

06446+0029. There are at least five features over a velocity range of over 7 km s^{-1} . The feature at 48.6 km s^{-1} is the strongest one. There is near infrared emission in this region as seen in 2MASS, and a non-detection of SiO masers (Harju et al. 1998).

18319-0802. There are several features spanning a velocity range over 15 km s^{-1} . The weakest feature is only about 0.2 Jy. An ultracompact (UC) HII region, separated by about $40''$, could be associated with this region (Becker et al. 1994).

18355-0650. There are at least five features spanning a velocity range of about 6 km s^{-1} . An UC HII region, separated by $17''$, is associated with this region (Becker et al. 1994).

G29.91-0.05 Features span from 93.4 to 105.3 km s^{-1} with multiple features being blended together. There are at least two compact HII regions associated with this region within $2'$ (Wood & Churchwell 1989a; Becker et al. 1994). One of them, separated by about $80''$, could be associated with this region.

18403-0440. This source primarily shows a single feature at $+20.1 \text{ km s}^{-1}$. No observations have been reported on this region, except near infrared emission from the 2MASS.

18479-0005. Walsh et al. (1997) did not detect maser emission within their 1 Jy limit (3σ). There are several features crowded within a velocity range of only 2 km s^{-1} . A UC HII region is associated with this source (Kurtz et al. 1994).

20275+4001. This source displays a single feature at -6.9 km s^{-1} , which matches the H^{13}CO^+ (4-3) peak of Hasegawa & Mitchell (1995). A bipolar outflow and a continuum source were also detected in this region (Hasegawa & Mitchell 1995; Trinidad et al. 2003). Mid-infrared images show that this source is surrounded by an optically thick dusty envelope (Marengo et al. 2000).

21306+5540. There are clearly five features in this source. Except for near infrared emission from the 2MASS, no other observations have reported in this region.

22176+6303 (S140). This source shows a double peaked structure and is the weakest source detected in this survey. At a distance of 910 pc (Crampton & Fisher 1974), the maser luminosity is very low ($1.1 \cdot 10^{-9} L_\odot$). However, its infrared luminosity indicates that it is still associated with a massive star forming region (Table 2). A faint continuum source (Kurtz et al. 1994) and a CO

outflow (Minchin et al. 1993) are associated with the region.

4. Discussion

We detected 10 methanol masers from targeting 89 sources which results in a detection rate of $\sim 11\%$. However, to compare the statistics of H_2O and methanol masers, we have to consider the entire original sample of 178 sources that satisfied our selection criteria ($\delta \geq -10^\circ$). 47 sources have previous detections of methanol masers, while 42 sources were not observed due to constraints of observing time. Hence, the overall detection rate of methanol masers in a water maser sample is at least $\sim 32\%$. Our sample includes 17 sources that are associated with low-mass YSOs and 10 of them were observed in this survey. A nil detection rate from these sources adds to the results of Minier et al. (2003), suggesting that 6.7 GHz methanol masers are only associated with massive star forming regions. Therefore, excluding the low-mass YSOs, the detection rate is at least $\sim 35\%$.

Fig. 2 shows the color-color diagram of the IRAS sources associated with the sample of water masers. The box on the upper right corner shows the Wood & Churchwell (1989b) (hereafter WC) criteria used to identify embedded massive stars and ultracompact HII regions. The stars and circles show the old and new methanol maser detections respectively. 113 out of 154 sources satisfy the WC criteria, of which 40 sources have methanol maser emission. Since 21 sources satisfying the WC criteria were not observed, the detection rate among IRAS sources satisfying WC criteria and hosting H_2O masers is at least $\sim 35\%$. This detection rate is better than that of a survey based purely on IRAS sources satisfying WC criteria (e.g. see discussion of Ellingsen et al. 1996). It is to be cautioned that not all of these cases are true associations, as the IRAS source may point to the brightest far infrared source in the star forming region, and better positions for methanol masers may preclude some of the current associations (Ellingsen 2006; Pandian & Goldsmith 2007). There are also 12 methanol masers whose IRAS colors do not satisfy WC criteria. It can also be seen from Fig. 2 that there is no distinction between the IRAS sources associated with the new detections, and those associated with the previous detections (which are brighter), nor is there any distinction between the colors of sources with and without methanol masers. Thus, the low detection rate in our survey (11 %) is not due to any systematic differences between in the infrared properties of the sources in our survey (versus the sources associated with previous detections of methanol masers). The lack of distinction of the IRAS source properties of bright versus faint methanol masers is also consistent with the observation of Pandian & Goldsmith (2007).

There is only one detection with a peak flux density less than 1 Jy, (this is also the only such source in the entire sample including previous detections). It should be noted that our sample is not from an unbiased survey, and

hence it is not possible to discuss the implications of this in the context of the methanol maser population in the Galaxy. However, we note that this is consistent with the results of the simulation of van der Walt (2005) and the results of the Pandian et al. (2007). van der Walt (2005) using Monte Carlo simulations determined the completeness of surveys as a function of their flux densities, while the observational results of Pandian et al. (2007) corroborate the theoretical analysis with regard to the total number of methanol masers in the Galaxy. Moreover, Pandian et al. (2007) found that the distribution of peak flux densities drops at flux densities below ~ 1 Jy. This could be one of the reasons why we didn't detect many sources below 1 Jy. Fig. 3a (left panel) shows the luminosity distributions for both maser types as a function of the infrared luminosity of the host IRAS sources and Fig. 3b (right panel) shows the the maser luminosities of the two species plotted against each other. Only sources that show emission in both species are shown in Fig. 3. The infrared flux F_{IR} (used to determine the infrared luminosity L_{IR}) is calculated using the formula below (Casoli et al. 1986).

$$F_{IR}(10^{-13}\text{Wm}^{-2}) = 1.75\left(\frac{F_{12}}{0.79} + \frac{F_{25}}{2} + \frac{F_{60}}{3.9} + \frac{F_{100}}{9.9}\right) \quad (1)$$

where F_{12} , F_{25} , F_{60} and F_{100} refer to the IRAS fluxes in 12, 25, 60 and 100 μm respectively. The distances are taken from the literature. For sources with no published distance, the near kinematic distance, computed from the peak velocity of 6.7 GHz emission using the galactic rotation curve of Wouterloot & Brand (1989), assuming $R_0 = 8.5$ kpc and $\Theta_0 = 220$ km s $^{-1}$, is adopted. The near kinematic distance is used because it seems realistic (Sobolev et al. 2005).

Fig. 3a shows that there is reasonably good correlation seen between the infrared luminosity and that of both H_2O (Correlation coefficient $R = 0.64$, Probability $p < 0.0001$) and CH_3OH masers ($R = 0.56$, $p < 0.0001$). This correlation has been found in the past by a number of groups (e.g. Wouterloot & Walmsley 1986; Szymczak et al. 2005), and the vertical scatter is normally attributed to the variability of the masers. However, it is not clear as to whether this correlation is physically meaningful. On the one hand, both maser types are spatially separated and have very different excitation requirements. H_2O masers are collisionally pumped and occur in shocks along outflows, while CH_3OH masers produced by radiative pumping and originate from circumstellar disks or envelopes. Thus, it is not clear whether the correlation seen in Fig. 3a arises from a physical connection between the far-infrared luminosity and maser luminosity. Fig. 3b shows that there is also a good correlation between methanol and water maser luminosities ($R = 0.63$, $p < 0.0001$). Since there is no physical connection between the two quantities, it is possible that the correlations are just a distance squared effect, as suggested by Palla et al. (1991) for the correlation between the water maser and the infrared luminosity. It is also curious that the water masers in our sample (that are associated with methanol masers) are an order of magnitude

more luminous than the ones associated with the methanol maser sample of Szymczak et al. (2005). Some methanol masers detected in our survey have low luminosities with the faintest source having a maser luminosity of only $10^{-9} L_{\odot}$. However, the infrared luminosities of all sources range from 10^3 to $10^6 L_{\odot}$, indicating that they are associated with massive star formation.

5. Summary

A survey for 6.7 GHz CH₃OH masers was carried out toward 89 water masers and 10 new sources were detected, five of which are located beyond the solar circle. A nil detection rate from low-mass star forming regions enhances the conclusion that 6.7 GHz methanol masers are only associated with massive star forming regions. There is only one source maser with a peak flux density less than 1 Jy, which could be due to the nature of the methanol maser luminosity function. This paper presents only the results of the survey. In a separate paper, we will report on the environment around the masers, using ongoing observations of various molecules such as CO, HCO⁺, CN and NH₃. This will also elucidate on any differences between faint masers and their bright counterparts.

Acknowledgements. We would like to thank the anonymous referee for many useful suggestions and comments, which improved this paper. This research is supported by NSFC under grants 10673024, 10733030, 10703010 and 10621303, and NBRPC (973 Program) under grant 2007CB815403.

References

- Anglada, G., Estalella, R., and Pastor, J. et al., 1996, ApJ, 463, 205
- Becker, Robert H., White, Richard L., Helfand, David J., & Zoonematkermani, S., 1994, ApJS, 91, 347
- Beuther, H., Walsh, A., Schilke, P., Sridharan, T. K., Menten, K. M., & Wyrowski, F., 2002, A&A, 390, 289
- Brand, J., Cesaroni, R., Caselli, P., et al. 1994, A&AS, 103, 541
- Breen, S. L., Ellingsen, S. P., & Johnston-Hollitt, M. et al., 2007, MNRAS, 377, 491
- Breckenridge, S. M., & Kukulich, S. G. 1995, ApJ, 438, 504
- Casoli F., Dupraz C., Gerin M., Combes F., Boulanger F. 1986, A&A 169, 281
- Caswell, J. L., Vaile, R. A., Ellingsen, S. P., Whiteoak, J. B., & Norris, R. P, 1995, MNRAS, 272, 96
- Codella, C., & Moscadelli, L., 2000, A&A, 362, 723
- Comoretto, G., Palagi, F., Cesaroni, R., et al. 1990, A&AS, 84, 179
- Crampton, D., & Fisher, W. A., 1974, Pub. Dom. Astrophys. Obs., 14, 283
- Ellingsen, S. P. 2006, ApJ, 638, 241
- Ellingsen, S. P. 2007, MNRAS, 377, 571
- Ellingsen, S. P., von Bibra, M. L., McCulloch, P. M., Norris, R. P., Deshpande, A. A., & Phillips, C. J. 1996, MNRAS, 280, 378
- Harju, J., Lehtinen, K., Booth, R. S., & Zinchenko, I., 1998, A&AS, 132, 211
- Hasegawa, T. I., & Mitchell, G. F. 1995, ApJ, 451, 225
- Kurtz, S., Churchwell, E., & Wood, D. O. S., 1994, ApJS, 91, 659
- Malyshev, A. V., & Sobolev, A. M., 2003, A&AT, 22, 1
- Marengo, M., Jayawardhana, R., & Fazio, G. G. et al., 2000, ApJ, 541, L63
- Minier, V., Ellingsen, S. P., Norris, R. P., & Booth, R. S., 2003, A&A, 403, 1095
- Minchin, N. R., White, G. J., & Padman, R, 1993, A&A, 277, 595
- Molinari, S., Testi, L., Rodríguez, L. F., & Zhang, Q., 2002, ApJ, 570, 758
- Ott, M., Witzel, A., & Quirrenbach, A., 1994, A&A, 284, 331
- Palagi, F., Cesaroni, R., and Comoretto, G. et al, 1993, A&AS, 101, 153
- Palla F., Brand J., Cesaroni R. et al., 1991, A&A 246, 249
- Pandian, J. D., & Goldsmith, P. F. 2007, ApJ, 669, 435
- Pandian, J. D., Goldsmith, P. F., & Deshpande, A. A. 2007, ApJ, 656, 255
- Pestalozzi M., Minier V. & Booth R. 2005, A&A, 432, 737
- Sobolev, A. M., Ostrovskii, A. B., Kirsanova, M. S. et al. 2005, IAUS, 227, 174
- Szymczak, M., Pillai, T., & Menten, K. M., 2005, A&A, 434, 613
- Szymczak, M., Kus, A. J., Hrynek, G., Kepa, A., & Pazderski, E. 2002, A&A, 392, 277
- Szymczak, M., Hrynek, G., & Kus, A. J., 2000, A&AS, 143, 269
- Trinidad, M. A., Curiel, S., Cantó, J. et al., 2003, ApJ, 589, 386
- van der Tak F., van Dishoeck E. F., Evans II N.J. et al, 1999, ApJ, 522, 991
- van der Walt, J., 2005, MNRAS, 360, 153
- Walsh, A. J., Hyland, A. R., Robinson, G., & Burton, M. G, 1997, MNRAS, 291, 261
- Wood, D. O. S., & Churchwell, E, 1989a, ApJS, 69, 831
- Wood, D. O. S., & Churchwell, E, 1989b, ApJ, 340, 265
- Wouterloot, J. G. A., Brand, J., 1989, A&AS, 80, 149
- Wouterloot, J. G. A., Brand, J., Fiegle, K., 1993, A&AS, 98, 589
- Wouterloot, J. G. A., & Walmsley, C. M., 1986, A&A, 168, 237
- Wu, Y., Zhang, Q., Yu, W. et al., 2006, A&A, 450, 607
- Xu, Y., Reid, M. J., Zheng, X. W., & Menten, K. M. 2006, Science, 311, 54
- Xu, Y., Zheng X. W., & Jiang, D. R. 2003, Chinese J. Astron. Astrophys., 3, 49

Table 1: The target sample of H₂O maser sources.

00211 + 6549	00259 + 5625 ^{ξ†}	00420 + 5530	00494 + 5617*	01134 + 6429	W3(1)
02219 + 6152*	W3(3) ^ξ	02232 + 6138*	02395 + 6244	02425 + 6851 [†]	02485 + 6902 [†]
03101 + 5821	03167 + 5848	03225 + 3034 [†]	03245 + 3002 [†]	04579 + 4703	05137 + 3919**
05168 + 3634 ^ξ	05274 + 3345*	05302 – 0537 ^{ξ†}	05327 – 0457 ^ξ	KLIRC2 ^ξ	05329 – 0508 ^{ξ†}
05329 – 0512 [†]	05335 + 3609	05345 + 3556	05345 + 3157	05358 + 3543*	05361 + 3539
05363 + 2454	05375 + 3540 ^ξ	NGC2024 ^ξ	05445 + 0020 [†]	05466 + 2316 ^{ξ†}	05553 + 1631
06001 + 3014 ^{ξ†}	MONR2 ^ξ	06053 – 0622*	06055 + 2039*	06058 + 2138*	06061 + 2151*
06067 + 2138 [†]	06099 + 1800*	06117 + 1350*	06127 + 1418	06291 + 0421	06306 + 0437 [†]
06437 + 0009	06446 + 0029**	06501 + 0143	06579 – 0432 [†]	06584 – 0852 ^ξ	07006 – 0654
18265 + 0028 [†]	18282 – 0951*	18290 – 0924*	18316 – 0602*	18319 – 0802**	G23.44 – 0.18*
G23.01 – 0.41*	OH24.7 + 0.2	18335 – 0713*	18341 – 0727*	18355 – 0650**	18359 – 0334
18360 – 0537	18385 – 0512	18403 – 0440**	18411 – 0338*	18434 – 0242*	G29.91 – 0.05**
18449 – 0115*	W43(M2) ^ξ	18450 – 0148 ^ξ	W43(M3)*	18455 – 0200	18461 – 0136
18469 – 0132	18469 – 0041	18470 – 0049*	18479 – 0005**	18487 – 0015*	18507 + 0121*
18507 + 0110*	18517 + 0437*	S76W	18537 + 0749	18538 + 0216 ^ξ	G35.05 – 0.52 ^ξ
18556 + 0136*	18581 + 0409 ^ξ	18585 + 0407 ^ξ	18592 + 0108*	18593 + 0408 ^ξ	19008 + 0530 ^ξ
19045 + 0813	19061 + 0652	19078 + 0901*	W49S ^ξ	19088 + 0902	19092 + 0841*
19095 + 0930*	19110 + 1045*	19181 + 1349	19207 + 1410	19209 + 1421	19213 + 1424*
19213 + 1723	W51M ^ξ	19287 + 1816 [†]	19287 + 1845 ^{ξ†}	19303 + 1651*	19363 + 2018
19374 + 2352	19388 + 2357*	19410 + 2336*	19433 + 2743 [†]	19474 + 2637	19598 + 3324
20050 + 2720 [†]	20056 + 3350	20062 + 3550*	20081 + 3122*	20110 + 3321*	20126 + 4104*
20144 + 3726	20160 + 3911 ^ξ	20188 + 3928 ^ξ	20198 + 3716*	ON2N	20215 + 3725 ^ξ
20227 + 4154 ^ξ	20231 + 3440 ^{ξ†}	20275 + 4001**	20286 + 4105 ^ξ	W75N*	W75S(1) ^ξ
W75OH ^ξ	W75S(3) ^ξ	21007 + 4951 ^{ξ†}	21008 + 4700	21078 + 5211 ^ξ	21144 + 5430
21173 + 5450	21206 + 5145 ^ξ	21228 + 5332	G97.53 + 3.19 ^ξ	21306 + 5540**	21307 + 5049
21334 + 5039	21368 + 5502	21379 + 5106	21381 + 5000*	21391 + 5026 ^ξ	21391 + 5802 [†]
21413 + 5442*	21418 + 6552	BFS11 – B	21479 + 5510 ^ξ	21527 + 5727	21553 + 5908
21558 + 5907	22142 + 5206	22176 + 6303**	22198 + 6336 [†]	22199 + 6322 [†]	22305 + 5803
22475 + 5939	22517 + 6215 [†]	22543 + 6145*	22570 + 5912 ^ξ	23004 + 5642	23004 + 5642
23030 + 5958 ^ξ	23116 + 6111*	S158 ^ξ	23138 + 5945		

*: Previously known methanol masers.

**: New detected methanol masers.

ξ: Not observed due to constraints of observing time.

†: Infrared luminosities less than 10³ L_⊙.

Table 2: Details of the newly detected 6.7 GHz CH₃OH masers. The first column lists the source name (associated IRAS source or the galactic coordinates). The next two columns give their J2000 equatorial coordinates. Col. (4) shows the distances. Cols. (5) and (6) present the integrated flux density and peak flux density. Cols. (7) and (8) show the radial velocity of peak emission and the radial velocity range. Cols. (9) - (11) present the infrared, CH₃OH and H₂O luminosities. The maser luminosities are calculated assuming isotropic emission.

Source Name	R.A.(2000) (^h ^m ^s)	DEC(2000) ([°] ['] ^{''})	D (kpc)	S_i (Jy km s ⁻¹)	S_p (Jy)	v_p (km s ⁻¹)	Δv (km s ⁻¹)	L_{IR} (L_{\odot})	L_{CH_3OH} (L_{\odot})	L_{H_2O} (L_{\odot})
05137 + 3919	05 17 13.3	+39 22 14	12.0 ¹	0.7	1.5	-16.2	-21.1,-16.0	6.1(4)	7.0(-7)	2.2(-4)
06446 + 0029	06 47 12.9	+00 26 07	6.0 ¹	2.8	1.6	48.6	42.7, 50.0	2.3(4)	7.0(-7)	1.5(-4)
18319 - 0802	18 34 38.2	-07 59 35	2.8*	2.2	2.1	35.7	31.0, 45.2	7.2(3)	1.2(-7)	4.5(-6)
18355 - 0650	18 38 14.3	-06 47 47	5.7 ⁴	4.2	3.9	58.2	56.6, 62.1	7.4(5)	9.4(-7)	7.1(-6)
18403 - 0440	18 43 01.1	-04 36 41	3.3 ⁴	0.3	1.0	20.1	19.8, 20.4	4.1(3)	2.3(-8)	3.2(-6)
G29.91 - 0.05	18 46 05.9	-02 42 27	7.1*	7.8	2.9	104.3	93.4, 105.3	— — —	2.7(-6)	3.3(-5)
18479 - 0005	18 50 31.1	-00 01 54	13.0 ²	1.3	1.5	27.4	24.9, 28.3	1.6(6)	1.5(-6)	9.0(-5)
20275 + 4001	20 29 24.9	+40 11 21	2.0 ³	1.7	4.0	-6.9	-7.4,-6.5	6.7(4)	4.7(-8)	1.5(-5)
21306 + 5540	21 32 13.0	+55 52 56	8.6 ¹	1.5	1.1	-69.9	-73.7,-68.0	1.4(5)	7.8(-7)	9.9(-4)
22176 + 6303	22 19 18.3	+63 18 48	0.9 ⁶	0.2	0.5	-2.0	-2.3,-1.1	2.4(4)	1.1(-9)	4.8(-7)

References for the distances:

1 Wouterloot et al. 1993. 2 Palagi et al 1993. 3 Anglada et al. 1996. 4 van der Tak et al. 1999. 5 Wu et al. 2006. 6 Crampton & Fisher 1974

* Heliocentric near kinematic distances.

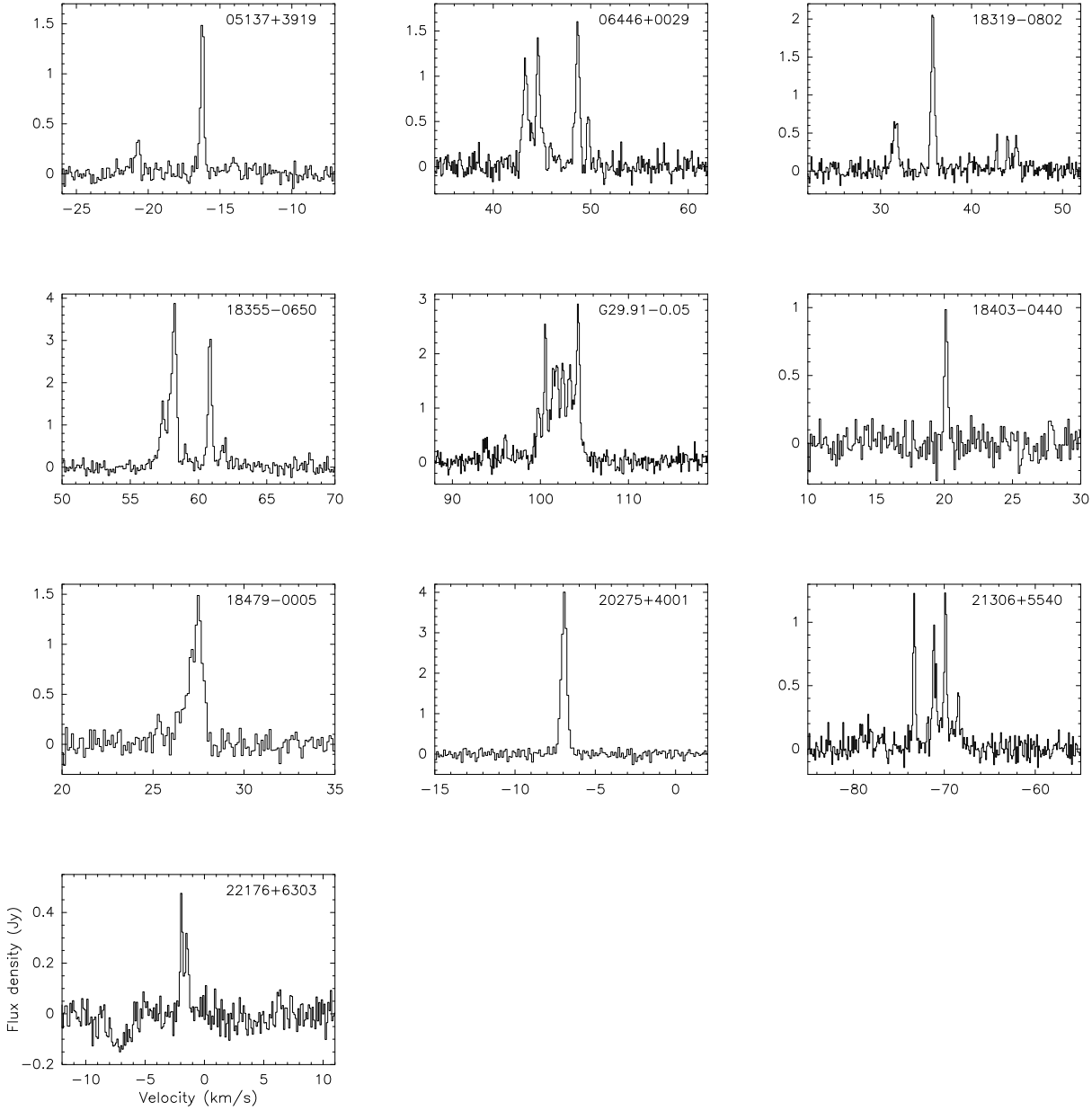


Fig. 1. Spectra of the new 6.7-GHz CH_3OH maser detections. The spectral resolution is 0.11 km s^{-1} .

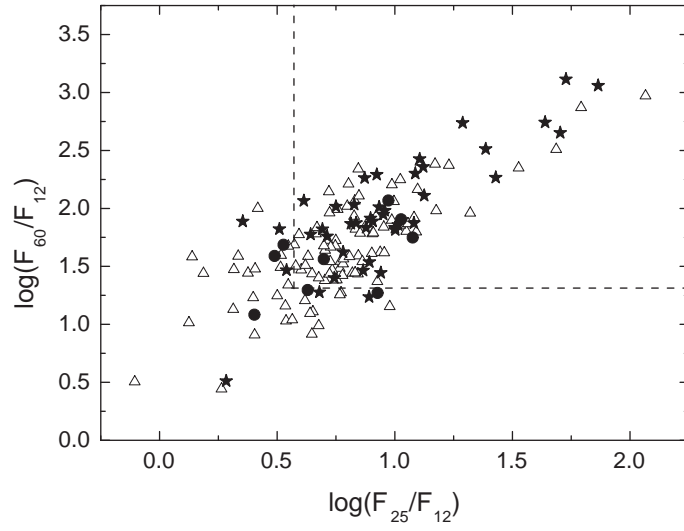


Fig. 2. IRAS color-color diagram for 154 sources. The box in the upper right corner delineates the WC criteria for UCHII regions. Sources with no methanol maser detections are shown in open triangles. Previous and new detections of methanol masers are shown in stars and circles respectively.

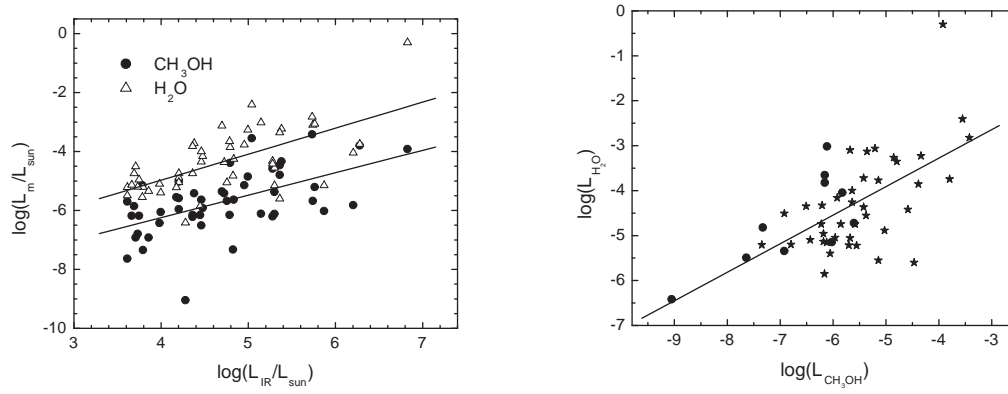


Fig. 3. Left panel – (a) Methanol and water maser luminosities versus the infrared luminosity calculated from the IRAS data. The circles and triangles show the methanol and water masers respectively. Water masers without any methanol maser associations are excluded. Right panel – (b) Water maser versus methanol maser luminosity. Previous and new detections of methanol masers are shown in stars and circles respectively.

6. Online Material

Table 3: H₂O maser sources that have non detections for 6.7 GHz CH₃OH maser emission. The columns show the source name, J2000 coordinates, central velocity for the spectrometer, v_c , velocity range covered by the spectrometer, v_{min} and v_{max} , the velocity resolution, $\delta(v)$, and the rms noise in the spectrum (1σ limit on the maser flux density).

Source Name	R.A.(2000) (^h ^m ^s)	DEC(2000) ([°] ['] ^{''})	v_c (km s ⁻¹)	v_{min} (km s ⁻¹)	v_{max} (km s ⁻¹)	$\delta(v)$ (km s ⁻¹)	RMS (Jy)
00211 + 6549	00 23 58.1	+66 06 03	-71.1	-296	154	0.11	0.14
00420 + 5530	00 44 57.5	+55 47 18	-47.8	-273	177	0.11	0.14
01134 + 6429	01 16 47.2	+64 45 39	-46.9	-272	178	0.11	0.10
W3(1)	02 25 28.2	+62 06 58	-40.0	-265	185	0.11	0.10
02395 + 6244	02 43 29.1	+62 57 00	-67.1	-292	158	0.11	0.10
02425 + 6851	02 47 00.2	+69 04 11	-10.4	-461	440	0.22	0.05
02485 + 6902	02 53 07.2	+69 14 36	-10.4	-461	440	0.22	0.05
03101 + 5821	03 14 04.7	+58 33 08	-38.5	-489	412	0.22	0.05
03167 + 5848	03 20 44.3	+58 59 33	-55.6	-506	395	0.22	0.05
03225 + 3034	03 25 35.5	+30 45 21	2.6	-223	228	0.11	0.19
03245 + 3002	03 27 39.0	+30 13 00	4.4	-446	455	0.22	0.05
04579 + 4703	05 01 39.7	+47 07 23	-17.8	-243	207	0.11	0.10
05329 - 0512	05 35 27.5	-05 09 37	7.5	-218	233	0.11	0.19
05335 + 3609	05 36 52.5	+36 10 49	-17.3	-468	433	0.22	0.05
05345 + 3556	05 37 57.8	+35 58 41	-20.7	-471	430	0.22	0.05
05345 + 3157	05 37 53.1	+31 59 35	-20.0	-245	205	0.11	0.19
05361 + 3539	05 39 27.7	+35 40 43	-18.0	-469	433	0.22	0.05
05363 + 2454	05 39 28.2	+24 56 32	13.9	-437	464	0.22	0.05
05445 + 0020	05 47 05.4	+00 21 50	15.9	-209	241	0.11	0.19
05553 + 1631	05 58 13.9	+16 32 00	-7.6	-233	218	0.11	0.14
06067 + 2138	06 09 48.0	+21 38 11	3.2	-447	454	0.22	0.05
06127 + 1418	06 15 34.6	+14 17 10	11.3	-214	237	0.11	0.19
06291 + 0421	06 31 48.1	+04 19 31	9.6	-216	235	0.11	0.19
06306 + 0437	06 33 16.4	+04 34 57	10.1	-440	461	0.22	0.05
06437 + 0009	06 46 15.6	+00 06 19	33.6	-192	259	0.11	0.19
06501 + 0143	06 52 45.6	+01 40 15	52.0	-399	503	0.22	0.05
06579 - 0432	07 00 23.1	-04 36 38	26.3	-424	477	0.22	0.05
07006 - 0654	07 03 05.1	-06 58 28	29.1	-421	480	0.22	0.05
18265 + 0028	18 29 05.8	+00 30 36	5.3	-220	231	0.11	0.19
OH24.7 + 0.2	18 35 29.9	-07 13 10	25.9	-199	251	0.11	0.14
18359 - 0334	18 38 34.3	-03 32 06	-45.5	-271	180	0.11	0.14
18360 - 0537	18 38 41.6	-05 35 06	104.4	-121	330	0.11	0.19

Table 1-continued

Source Name	R.A.(2000) (^h ^m ^s)	DEC(2000) ([°] ['] ^{''})	v_c (km s ⁻¹)	v_{min} (km s ⁻¹)	v_{max} (km s ⁻¹)	$\delta(v)$ (km s ⁻¹)	RMS (Jy)
18385 - 0512	18 41 12.0	-05 09 07	18.0	-207	243	0.11	0.24
18455 - 0200	18 48 08.8	-01 56 54	104.3	-130	320	0.11	0.19
18461 - 0136	18 48 45.2	-01 33 12	18.6	-207	244	0.11	0.19
18469 - 0132	18 49 32.8	-01 29 04	93.6	-132	319	0.11	0.24
18469 - 0041	18 49 32.2	-00 38 01	92.5	-133	318	0.11	0.19
<i>S76W</i>	18 55 58.7	+07 53 42	-3.6	-229	222	0.11	0.19
18537 + 0749	18 56 11.8	+07 53 24	31.7	-194	257	0.11	0.19
19045 + 0813	19 06 59.7	+08 18 42	16.9	-208	242	0.11	0.19
19061 + 0652	19 08 36.8	+06 57 02	71.9	-153	297	0.11	0.19
19088 + 0902	19 11 15.8	+09 07 27	-5.1	-230	220	0.11	0.19
19181 + 1349	19 20 31.2	+13 55 24	34.1	-191	259	0.11	0.19
19207 + 1410	19 23 01.2	+14 16 40	68.6	-157	294	0.11	0.29
19209 + 1421	19 23 10.9	+14 26 38	52.1	-173	277	0.11	0.24
19213 + 1723	19 23 37.0	+17 28 59	-26.8	-252	198	0.11	0.14
19287 + 1816	19 30 58.3	+18 22 28	24.5	-201	250	0.11	0.19
19363 + 2018	19 38 31.6	+20 25 21	36.0	-189	261	0.11	0.19
19374 + 2352	19 39 33.2	+23 59 55	39.4	-186	265	0.11	0.19
19433 + 2743	19 45 20.8	+27 50 51	19.9	-205	245	0.11	0.19
19474 + 2637	19 49 32.5	+26 45 14	20.5	-205	246	0.11	0.19
19598 + 3324	20 01 45.5	+33 32 41	-19.4	-245	206	0.11	0.24
20050 + 2720	20 07 06.7	+27 28 53	0.9	-224	226	0.11	0.19
20056 + 3350	20 07 31.5	+33 59 39	10.4	-215	236	0.11	0.19
20144 + 3726	20 16 15.8	+37 35 40	-56.7	-507	394	0.22	0.05
<i>ON2N</i>	20 21 43.9	+37 26 39	2.4	-448	453	0.22	0.05
21008 + 4700	21 02 32.3	+47 12 36	-49.6	-500	401	0.22	0.05
21144 + 5430	21 15 55.8	+54 43 31	-83.2	-534	367	0.22	0.05
21173 + 5450	21 18 53.1	+55 03 19	-82.8	-533	368	0.22	0.05
21228 + 5332	21 24 29.0	+53 45 34	-97.4	-548	353	0.22	0.05
21307 + 5049	21 32 31.4	+51 02 23	-46.7	-272	179	0.11	0.10
21334 + 5039	21 35 09.1	+50 53 09	-43.9	-269	181	0.11	0.19
21368 + 5502	21 38 25.8	+55 16 33	-83.2	-308	142	0.11	0.19
21379 + 5106	21 39 40.5	+51 20 32	-41.6	-267	184	0.11	0.19
21391 + 5802	21 40 42.3	+58 16 10	-5.0	-230	220	0.11	0.10
21418 + 6552	21 43 04.0	+66 05 57	-31.2	-256	194	0.11	0.10
<i>BFS11 - B</i>	21 43 06.0	+66 06 57	-14.9	-240	210	0.11	0.05
21527 + 5727	21 54 21.5	+57 41 14	-70.3	-296	155	0.11	0.10
21553 + 5908	21 56 59.3	+59 22 39	-87.8	-538	363	0.22	0.05
21558 + 5907	21 57 24.5	+59 21 56	-89.6	-315	136	0.11	0.05
22142 + 5206	22 16 10.4	+52 21 25	-37.4	-488	413	0.22	0.05
22198 + 6336	22 21 27.5	+63 51 46	-21.3	-247	204	0.11	0.10
22199 + 6322	22 21 33.2	+63 37 22	-9.0	-460	442	0.22	0.05
22305 + 5803	22 32 24.2	+58 18 58	-53.0	-278	172	0.11	0.19
22475 + 5939	22 49 29.5	+59 55 37	-54.5	-280	171	0.11	0.10
22517 + 6215	22 53 43.4	+62 31 46	-9.0	-234	216	0.11	0.19
23004 + 5642	23 02 34.9	+56 58 55	-53.5	-504	397	0.22	0.05
23004 + 5642	23 02 32.1	+56 57 51	-53.5	-279	172	0.11	0.19
23138 + 5945	23 16 04.4	+60 01 34	-44.5	-270	181	0.11	0.19